NAVAL POSTGRADUATE SCHOOL

Monterey, California

THESIS

DEVELOPMENT AND TESTING OF A PROTOTYPE ELECTRO-OPTICAL PHASE ENCODED POSITION TRANSDUCER

by

Gary R. Parriott
December 1991

Thesis Advisor : David S. Davis

Approved for public release; distribution is unlimited

SECURITY CLASSIFICATION OF THIS PAGE

REPORT DOCUMENTATION PAGE

1a. REPORT SECURITY CLASSIFICATION UNCLASSIFIED	1b. RESTRICTIVE MARKINGS
2a. SECURITY CLASSIFICATION AUTHORITY	3. DISTRIBUTION/AVAILABILITY OF REPORT Approved for public release; distribution is unlimited.
2b. DECLASSIFICATION/DOWNGRADING SCHEDULE	
4. PERFORMING ORGANIZATION REPORT NUMBER(S)	5. MONITORING ORGANIZATION REPORT NUMBER(S)
6a. NAME OF PERFORMING ORGANIZATION Naval Postgraduate School 6b. OFFICE SYMBOL (*If applicable*) 55	7a. NAME OF MONITORING ORGANIZATION Naval Postgraduate School
6c. ADDRESS (*City, State, and ZIP Code*) Monterey, CA 93943-5000	7b. ADDRESS (*City, State, and ZIP Code*) Monterey, CA 93943-5000
8a. NAME OF FUNDING/SPONSORING ORGANIZATION 8b. OFFICE SYMBOL (*If applicable*)	9. PROCUREMENT INSTRUMENT IDENTIFICATION NUMBER
8c. ADDRESS (*City, State, and ZIP Code*)	10. SOURCE OF FUNDING NUMBERS Program Element No / Project No / Task No / Work Unit Accession Number
11. TITLE (*Include Security Classification*) Testing and Development of a Prototype Electro-Optical Phase Encoded Transducer	
12. PERSONAL AUTHOR(S)	
13a. TYPE OF REPORT Master's Thesis 13b. TIME COVERED From To	14. DATE OF REPORT (*year, month, day*) December 1991 15. PAGE COUNT 61
16. SUPPLEMENTARY NOTATION The views expressed in this thesis are those of the author and do not reflect the official policy or position of the Department of Defense or the U.S. Government.	
17. COSATI CODES FIELD / GROUP / SUBGROUP	18. SUBJECT TERMS (*continue on reverse if necessary and identify by block number*) Phase encoded position transducer, Position encoder

19. ABSTRACT (*continue on reverse if necessary and identify by block number*)

A proof-of-concept experimental validation of a proposed idea for a prototype electro-optical phase encoded position transducer was conducted. The intensity of two IR LED beams were modulated sinusoidally at frequency w , with a 90 degree temporal phse difference. They were further modulated by a pair of sinusoidal optical encoding masks with a 90 degree spatial phase difference. The mask pair was mounted on a mechanical stage and translated perpendicular to the beam axis. The sum of the two signals produced by this electro-optical configuration constituted another sinusoid at temporal frequency w, whose phase was proportional to the mask position. Although small deviations from ideal behavior were observed, the validity of the technique has been established incontestably.

20. DISTRIBUTION/AVAILABILITY OF ABSTRACT ☒ UNCLASSIFIED/UNLIMITED ☐ SAME AS REPORT ☐ DTIC USERS	21. ABSTRACT SECURITY CLASSIFICATION UNCLASSIFIED
22a. NAME OF RESPONSIBLE INDIVIDUAL David S. Davis	22b. TELEPHONE (*Include Area code*) (408) 646-2116 22c. OFFICE SYMBOL 61DV

DD FORM 1473, 84 MAR 83 APR edition may be used until exhausted
All other editions are obsolete

SECURITY CLASSIFICATION OF THIS PAGE
UNCLASSIFIED

Approved for public release: Distribution is unlimited

Developing and Testing of a Prototype Electro-Optical Phase Encoded Position Transducer

by

Gary R. Parriott
Lieutenant, United States Navy
B.S., Iowa State University, 1984

Submitted in partial fulfillment
of the requirements for the degree of

MASTER OF SCIENCE IN PHYSICS

from the

NAVAL POSTGRADUATE SCHOOL
December 1991

Author: 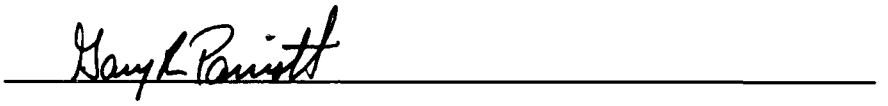

Gary R. Parriott

Approved by: 

D. S. Davis, Thesis Advisor

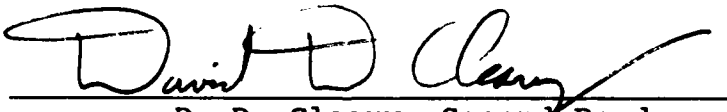

D. D. Cleary, Second Reader

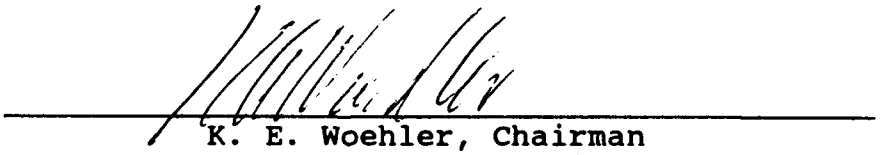

K. E. Woehler, Chairman
Department of Physics

ABSTRACT

A proof-of-concept experimental validation of a proposed idea for a prototype electro-optical phase encoded position transducer was conducted. The intensity of two IR LED beams were modulated sinusoidally at frequency ω, with a 90 degree temporal phase difference. They were further modulated by a pair of sinusoidal optical encoding masks with 90 degree spatial phase difference. The mask pair was mounted on a mechanical stage and translated perpendicular to the beam axis. The sum of the two signals produced by this electro-optical configuration constituted another sinusoid at temporal frequency ω, whose phase was proportional to the mask position. Although small deviations from ideal behavior were observed, the validity of the technique has been established incontestably.

TABLE OF CONTENTS

LIST OF FIGURES

I. INTRODUCTION

A. MOTIVATION

This thesis project is part of a larger research and development program to design and build a next generation middle infrared detection and imaging system by the author's advisor, D. S. Davis. Part of Davis' proposed technique is that a state-of-the-art imaging spectroscopic system can be developed using orthogonal Walsh functions to encode multiplexed images, thereby achieving extreme sensitivity [Ref. 1]. The validity of this technique was proven by R. H. McKenzie, Capt., USMC, in an earlier thesis [Ref. 2], and further investigated in a thesis by B. J. Musselman, LT., USCG, [Ref. 3].

This project stems from Davis' interest in spectroscopic research. He has previously designed a cryogenically cooled infrared multiplexing Fourier transform spectrometer, which is flown on NASA's Kuiper Airborne Observatory (KAO). Although the new instrument was initially proposed as a replacement for the current instrument to use on NASA's next generation airborne observatory SOFIA (Stratospheric Observatory For Infrared Astronomy), the technology should also be useful in other applications such as passive target surveillance detection and identification.

B. THESIS GOAL

Davis' technique requires the precise mechanical positioning of a pair of focal plane encoding masks, by means of an electro-optical servo system. Experience with previous generations of multiplexing instruments has determined that the best servo system performance is achieved with servo feedback signals that are phase-sensitive functions of loop error, rather than simple magnitude functions [Ref. 4, Ref. 5]. The goal of this thesis is to develop and to implement a proof-of-concept validation for such an electro-optical phase encoded position monitor, as it will be employed in the overall multiplexed imaging system.

The proposed system will be sensitive to the relative phases of a pair of amplitude-modulated IR beams. The intensity of the beams will be sinusoids with a 90° temporal phase difference, i.e., in quadrature, and modulated at frequency ω. They will be further modulated by a pair of sinusoidal optical encoding masks with 90° spatial phase difference. Let x represent the position of the masks. Then the optical configuration will produce two signals, one proportional to $\sin(\omega t)\sin(x)$ and the other to $\cos(\omega t)\cos(x)$. Their sum constitutes another sinusoidal signal at frequency ω, whose phase is just the mask position relative to some origin,

$$\cos(\omega t)\cos(x)+\sin(\omega t)\sin(x)=\cos(\omega t-x). \qquad (1)$$

Careful monitoring of the temporal phase difference between this signal (at frequency ω) and the original phase reference signal (also at frequency ω), should yield a phase difference that is linearly proportional to mask position. This system would allow for extremely accurate measurements of the mask position due to the precision with which phases can be measured. The position measurements would also have the advantage that they would not have the susceptibility to beam amplitude noise, such as that produced by power source fluctuations.

Figure 1 shows a block diagram overview of the project design. The electronics section consists of four main modules. The light sources module produces the quadrature sinusoid signals used for driving the LED emitters. The detector circuits convert the optical signals modulated by the optical masks to electronic signals. The signal processing circuits then sum the two output channels and filter out nonessential signal elements. Finally the phase comparator measures the relative phases between the reference (driving) signal and the summed output signal. The optical section consists of four positive lenses to focus the LEDs' output and the mask pair that modulates the light signals. Each of these elements is discussed in detail in the following chapters.

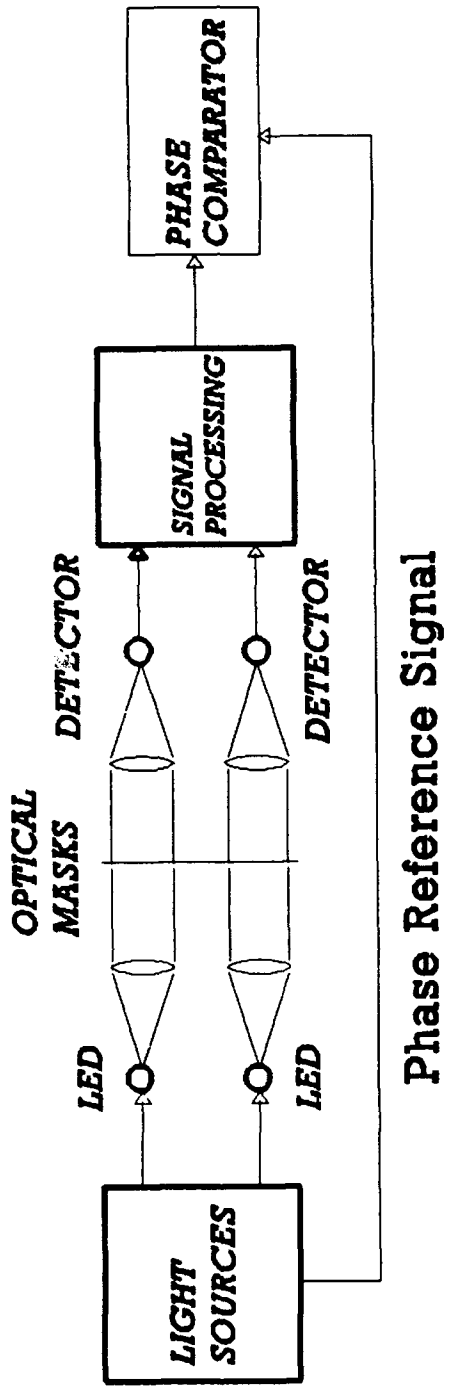

Figure 1 Block Diagram Overview of Proposed Thesis Project

II. ELECTRONICS

The electronic portion of the experimental setup consists of three parts, listed below and described in detail later in this chapter.

- Two-phase quadrature sinusoidal oscillator circuit.
- Optical detector circuit.
- Signal processing circuit.

A. OSCILLATOR CIRCUIT

1. LED

Drivers for the LED light sources were the first circuits to be constructed. Initially it was not known what modulation frequency would be required to achieve the best results, since the frequency bandwidth characteristics of the LEDs and detectors were not specified. In order to determine the optimum frequency experimentally, it was decided to drive a standard IR LED (peak wavelength λ=950nm) with a Tektronix CFG250 function generator and to measure the LED's frequency response. IR light sources were chosen instead of visible to allow working with the room lights on and to avoid 60 cycle pick-up from the room lights. It was found that the function generator had insufficient current drive capability to power the LED. Therefore, the output of the function generator fed

an emitter follower, which, in turn drove the LED. An emitter follower current amplifier, using a type 2N3053 NPN silicon transistor (component Q1 in Figure 2), was designed and constructed [Ref. 6:pp. 68-71].

The supply voltage for the emitter follower is +5V and is provided by a Texas Instruments uA7805c positive voltage regulator. The light source itself is an Archer SY-IR53L high intensity infrared LED. The LED requires a maximum sustained forward current of 20mA and a forward voltage of at least 1.3 VDC. This means that, theoretically, an external emitter resistance of at least 65Ω is needed for the LED to light without drawing excessive current. With the resistance used (R_{24} in Figure 2) the measured voltage drop across the LED was the required 1.3 VDC.

It is necessary to bias the follower's base to ensure that a collector current flows during the entire input signal swing. The simplest way to do this is with a voltage divider [Ref. 6:p. 70]. The 1.3 VDC drop across the LED combined with the internal 0.7 VDC drop across the transistor mandates that the base voltage be at least 2.0 VDC above ground. The negative swing of the source signal must also be accommodated, so the base voltage actually needs to be higher than 2.0 VDC. The values of the bias dividing resistors, R_{21} and R_{22}, were chosen to keep the measured base voltage at 3.4 VDC. The input resistance R_{19} and the load resistance R_{23} are chosen to

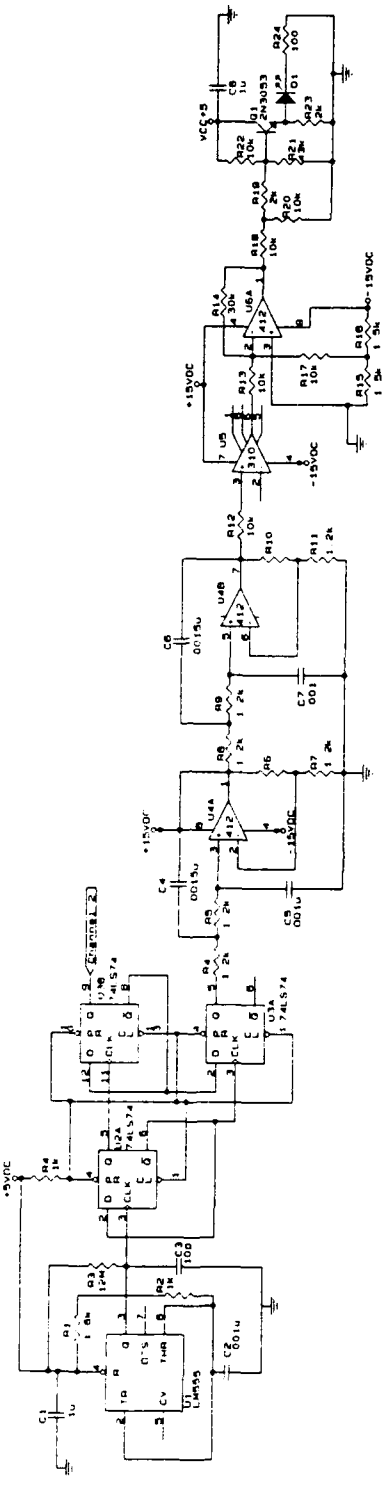

Figure 2 Light Source Schematic Drawing

be sufficiently small so that the effective impedance of the emitter follower is not established by the base biasing resistors.

2. OSCILLATOR

The two-phase oscillator that drives the LEDs in quadrature has to operate in the 70kHz to 125kHz frequency range. This range was determined by testing the frequency response of the LED/detector combination, as explained below in section II.B.3. Although there are several ways to produce two signals with the desired phases, a two-step method was chosen. The first step is to generate quadrature square waves using digital circuitry. The second step is to filter out the square waves' overtones using a low-pass filter, so that only the fundamental Fourier component, at the desired modulation frequency, remains. The details are described below.

a. Timer

The first component in Figure 2, U1, is the square wave generator, a Texas Instruments TLC555C timer chip, the operation of which is straightforward. Initially, when power is applied to the chip the output is HIGH, the charge on the capacitor is low, and the internal discharge transistor is off [Ref. 7:p. 171]. The capacitor then begins to charge through the series resistors R_1 and R_2 toward the supply voltage of +5V. When the capacitor gets to ⅔ V_{cc} (or 3.33 V) the threshold is triggered, causing the output to go LOW and

the discharge transistor to turn on [Ref. 6:pp. 286-287]. The capacitor is now discharged through resistor R_2 until the capacitor voltage drops to ⅓ V_{CC} (1.67 V). At this point the threshold triggers and returns the chip to its initial state. The operation is now cyclic with period $T=0.693(R_1+2R_2)C$. For the values shown, this gives a calculated frequency of 306kHz, and a measured frequency of 312kHz [Ref. 7:p. 47]. The measured frequency is approximately four times the desired operating frequency. This is necessary because subsequent production of the quadrature signals involves four-fold frequency division. This is described in detail in the next section.

b. Frequency Divider and Phase Shifter

The quadrature phase shift and frequency division are accomplished using two National Semiconductor DM74S74AN flip-flops (shown in Figure 2).

The rectangular pulse train A in Figure 3, at four times the desired frequency, is input from the TLC555C oscillator to the clock (CLK) input of U2A in Figure 2. Because the NOT Q output of U2A is tied to the D input, each positive leading edge of pulse train A toggles U2A to its alternate state. This produces the 50% duty cycle square wave B (Figure 3), at half the input frequency or twice the desired LED modulation frequency. The Q output is then fed to the clock of U3B. U3B is configured the same as U2A, so that its

Q output is the square wave C in Figure 3, at the desired modulation frequency. The NOT Q output of U2A is connected to the clock input of U3A, and therefore U3A responds to the negative going transition of pulse train B by passing the compliment of C to the Q output of U3A. However, the frequency of B is twice that of C, so that its negative going edges are phase shifted by one quarter cycle. This forces the square wave D (Figure 3) to lead pulse train C by 90 degrees.

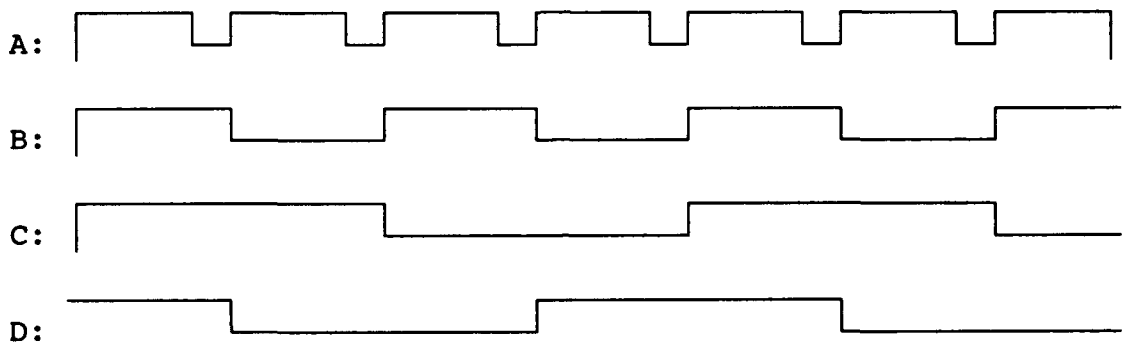

Figure 3 Square Wave Pulse Trains

c. Filter

Once quadrature square waves have been generated, the next stage is to filter out the overtones to produce a sine wave. This can be accomplished by passing the signal through a low pass active filter with a cutoff frequency, f_c, between f_{mod} and $2f_{mod}$, where f_{mod} is the desired LED modulation frequency. The Butterworth filter configuration was chosen

because it gives the flattest passband possible, combined with a reasonably fast initial falloff and moderate overshoot [Ref. 8:p. 72]. The design for the filter was adapted from Horowitz and Hill [Ref. 6:pp. 274-275] and consists of ICs U4A and U4B in Figure 2.

By cascading two filter sections together, the performance of the filter can be improved. The two sections of the filter are not identical but instead are designed so that each one contributes by adding its own cutoff frequency and damping as a quadratic factor of an *n*th-order polynomial describing the overall filter response [Ref 8:p. 18].

The frequency response properties of the filter are set by the input resistors $R_{4,5,8,9}$ and capacitors $C_{4,5,6,7}$, whose values are determined by $f_c=1/2\pi RC$. Resistors $R_{6,10}$ are determined from $R=(k_n-1)R_{5,9}$, where $k_6=1.152$, $k_{10}=2.235$ [Ref. 6:p. 274]. The resistors at the output of the op-amps provide a non-inverting voltage amplifier with gain $k_n=1+R_{6,10}/R_{7,11}$, where n is the filter stage. The values shown in the figure are for a cutoff frequency of f_c=100kHz. A National Semiconductor LF412 dual op-amp was used so that both stages of the filter could be included on one IC.

d. Offset Trim

The output signal from the two-phase oscillator is not yet sufficient to drive the LEDs. The characteristics of the signal and its DC offset do not match the output signal

from the function generator that drove an LED during the initial prototyping and testing discussed above in section A.1. By measuring the output of the function generator, as used during initial tests, it was concluded that the driving signal must have a voltage of 3 V_{pp} with a DC offset of 3.5 V. This was necessary to ensure operating in the linear range of the LED I-V curve. The output from the oscillator is $4V_{pp}$ with a 2 VDC offset. The easiest way to match the oscillator's output characteristics with the emitter follower requirements was to insert a non-inverting amplifier with a voltage divider at the summing point (U6A) in Figure 2. The resistors $R_{15,16}$ divide the applied -15 VDC signal by two. IC U6, which is an LM412 dual op-amp so that both channels can be accommodated on one chip, then amplifies the voltages with a gain of three, as determined by R_{13} and R_{14}. These two signals are added together and the voltage is further divided down to the required amplitude and offset by resistors $R_{18,20}$.

A unity gain amplifier (U5, Figure 2), using the LM310 unity gain buffer op-amp immediately upstream from the filter, isolates the amplifier from the oscillator. The resistor R_{12} is recommended by the manufacturer.

e. Completing the Circuit

After the successful prototyping of the two-phase oscillator, a more permanent version of the circuit was assembled on soldered circuit boards. The ICs were attached

to the circuit boards using solderless sockets. Pin-to-pin connections were made using above board soldered wire jumpers. The circuit boards were then screwed onto a plywood base with aluminum standoffs. The power supply leads from the circuit boards were connected to terminal blocks attached to the plywood base. A photograph of all the completed circuit boards is provided in Figure 4.

B. DETECTOR CIRCUIT

1. INITIAL DESIGN

The next phase of the development was the design of a matched pair of detector circuits. The main component of each circuit is a PIN photodiode. The initial design was simply to connect the detector to an inverting transimpedance amplifier using a LM301 op-amp. A gain greater than unity was required in order to ensure an output signal large enough to use downstream. The values of the input resistor R_1 and the feedback resistor R_2 were chosen so as to provide ample gain.

2. PROBLEMS/SOLUTIONS

The photodiode used for the detector has an internal impedance $Z \sim 10^6 \Omega$ when operated in the kilohertz range, increasing to $Z \sim 10^8 \Omega$ at lower frequencies. This allows a very small photocurrent to produce a large voltage (Ohm's Law). Consequently, the circuit is highly susceptible to unwanted electrostatic coupling as well as 60Hz pickup (magnetic coupling) from its surroundings [Ref 6:pp. 455-457].

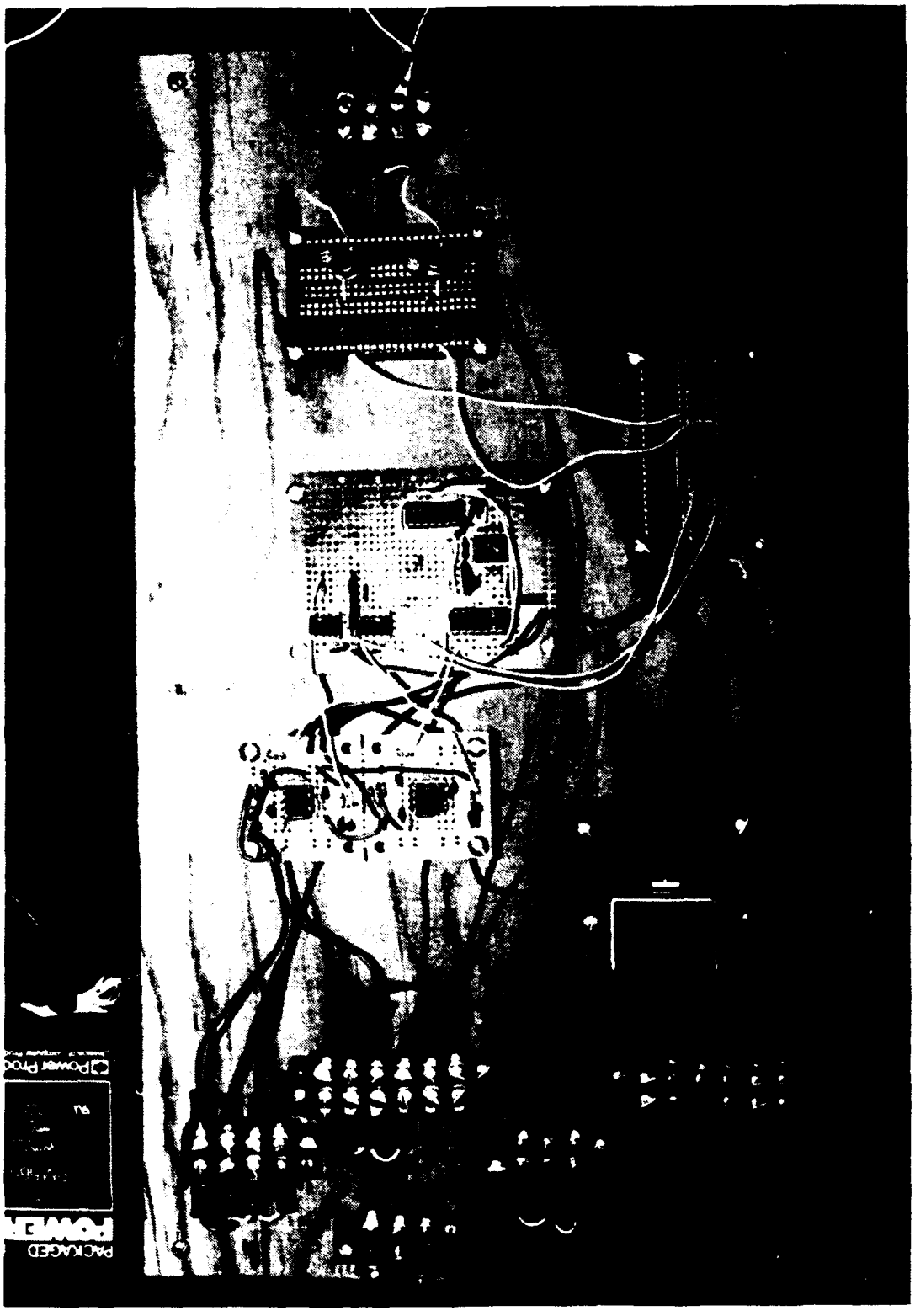

Figure 4 Photograph of Completed LED/Oscillator Circuit

A shielded box was built to help minimize coupling problems. The box consists of an aluminum casing with two apertures for the photodiodes and BNC connectors for the output. An internal aluminum plate placed immediately above the circuit board completes the shielding.

A shielded box however, does nothing to reduce the magnetic coupling. By using shielded twisted pair wire to connect the photodiodes to the op-amp, trimming the leads of the photodiodes as short as possible, and using twisted wire pairs to connect the op-amp output to the BNC connectors, pickup and interference are reduced to acceptable levels. Replacing the power supply with four 9V batteries, connected in series to provide ±18V to the circuit, added additional protection.

As a further precaution, a unity gain amplifier (U2, Figure 5), using an LM310 op-amp, was added between the inverting gain amplifiers and the BNC connectors to isolate the high impedance of the detector circuit from the downstream components.

3. TESTING

Once the circuit was completed, the next step was to test the LED/detector circuit to determine the best operating frequency. The detector output was connected to a Hewlett-Packard Fourier analyzer, while the LED was driven by a function generator which was set to frequency sweep mode.

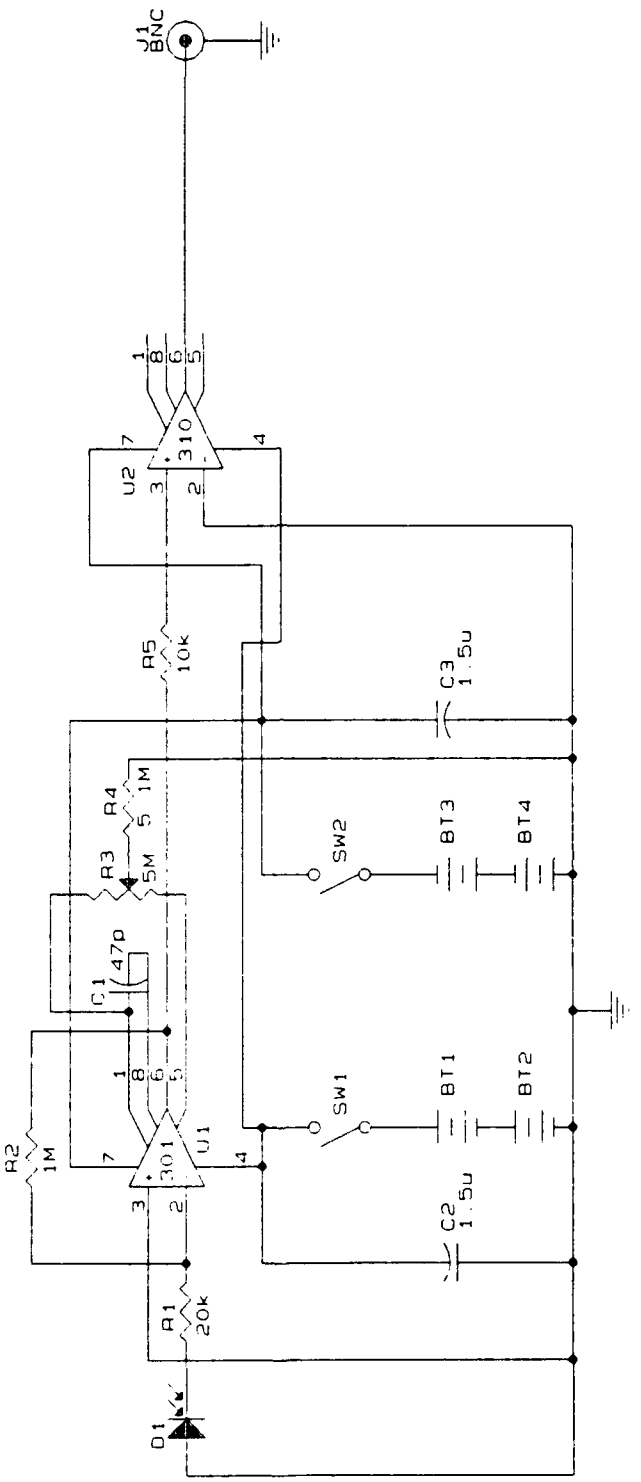

Figure 5 Detector Circuit Schematic Drawing

Overall LED/detector sensitivity was measured as a function of modulation frequency. This was necessary because the internal resistance and capacitance of the detector and the AC coupling effects of the low-pass filter combine to give an optimum frequency range. The results of the Fourier analysis established that the best operating frequency for the system was in the range between 70kHz and 125kHz.

C. SIGNAL PROCESSING

1. SUMMING AMPLIFIER

The main component in the signal processing section (Figure 6) is the summing amplifier (U1) that adds the two detector output signals in accordance with Equation (1). The input signals at this point must have the same amplitude in order to prevent scaling imbalance problems with the trigonometric identity (Equation (1)). Therefore, potentiometers are used for the input resistors R_1 and R_2 so that the gain of each signal can be adjusted as necessary.

The procedure for matching the signal gains was simple. With the input for channel two (the $\sin(\omega t)\sin(x)$ signal) grounded, the op-amp acted as a simple inverting gain amplifier for channel one ($\cos(\omega t)\cos(x)$ term) with gain of $-R_5/R_3+R_1$. The amplitude range was measured as R_1 was adjusted through its full range. The procedure was repeated for channel two. An output amplitude that was within both ranges

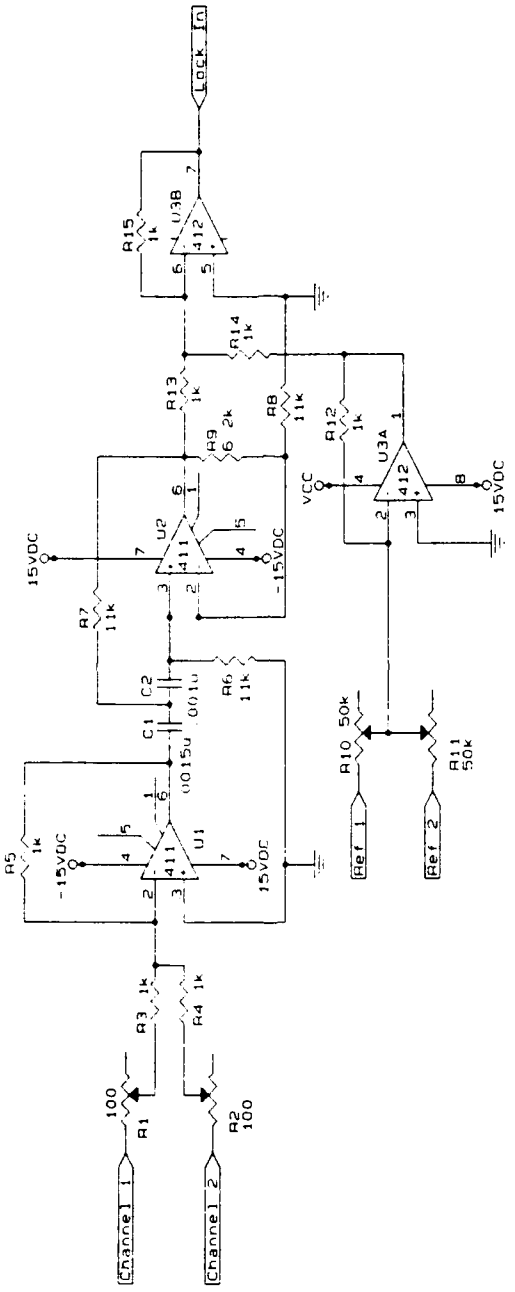

Figure 6 Signal Processing Schematic Drawing

was then chosen, and R_1 and R_2 were adjusted to provide the necessary gain.

2. HIGH PASS FILTER

The output of the above circuit needs to be further processed: there is DC term as well some low frequency terms that need to be filtered out. This was accomplished with a high-pass Butterworth filter. This filter is similar in design to the low-pass filter described previously, with the only difference being an interchange of resistors and capacitors. For this filter a two-pole design with any cutoff frequency below the modulation frequency f_{mod} will produce an acceptable response. The actual cutoff frequency chosen is f_c=15kHz.

3. FINAL PROCESSING

The final two components (U3A and U3B in Figure 6) in the signal processing circuit are summation amplifiers used to extract cos(ωt) and sin(ωt) terms from the signal output from U2. IC U3A has as its inputs the two reference signals driving the LEDs, with two potentiometers as the input resistors R_{10} and R_{11}. The potentiometers are adjusted for the correct gain and the voltages are summed. This signal cos(ωt)+sin(ωt) is then added to the output of the high-pass filter. The second summation amplifier is set for a gain of -1.

III. OPTICS

A. OPTICAL LAYOUT

1. COMPUTER GENERATED MASK

a. Mask Design

Once the electronic circuits were complete, the next phase was the optical design. The first optical problem was the design of a mask pair to modulate the two signal channels sinusoidally as a function of the mask's position. Both channels must be modulated simultaneously and in quadrature as the mask is translated.

The initial mask design was a sine wave spaced vertically 5cm above a cosine wave, with transparent areas between the curve and the x-axis and IR-opaque areas "outside" the curve. It was decided, however, that this design would not work because the detector would not recognize when the sine wave (or cosine) went negative. For example, as the mask was moved from $x=0$ to $x=\pi$, the intensity of the light that passed through the mask would increase from zero to a maximum value and then to zero again. As the mask moved from $x=\pi$ to $x=2\pi$ the intensity would follow the same pattern. In other words, the intensity would go from a minimum to a maximum back to a minimum in one-half cycle instead of one cycle, because

the detector signal was proportional to the inherently positive intensity of the detector.

A second mask was designed to give a DC offset by plotting the curve $A(1+\sin(\omega t))$, where the constant A is the amplitude of the curve. By allowing light to pass through the aperture defined by the curve and the x-axis, the intensity increases from a maximum value at $x=0$ through a minimum value and back to the maximum value at $x=2\pi$. A similar plot for the curve $A(1+\cos(\omega t))$ is drawn 5cm below the sine curve. An example of this design is presented in Figure 7. A pair of slits, vertically aligned, is then used to reduce the apparent area of the mask seen by the detector.

b. Computer Configuration

The program to create the optical mask described above was written on an IBM Personal System/2 Model 70 386 computer. The prototype encoding masks were drawn on a Hewlett-Packard model 7550A pen plotter connected to the IBM computer via a conventional 9600 baud RS-232 interface.

The C programming language was selected for the program development, based on the author's familiarity with that language. An additional contributing factor in the choice of language was the availability of the IBM-PC version of Turbo C++ 2.0 by Borland International.

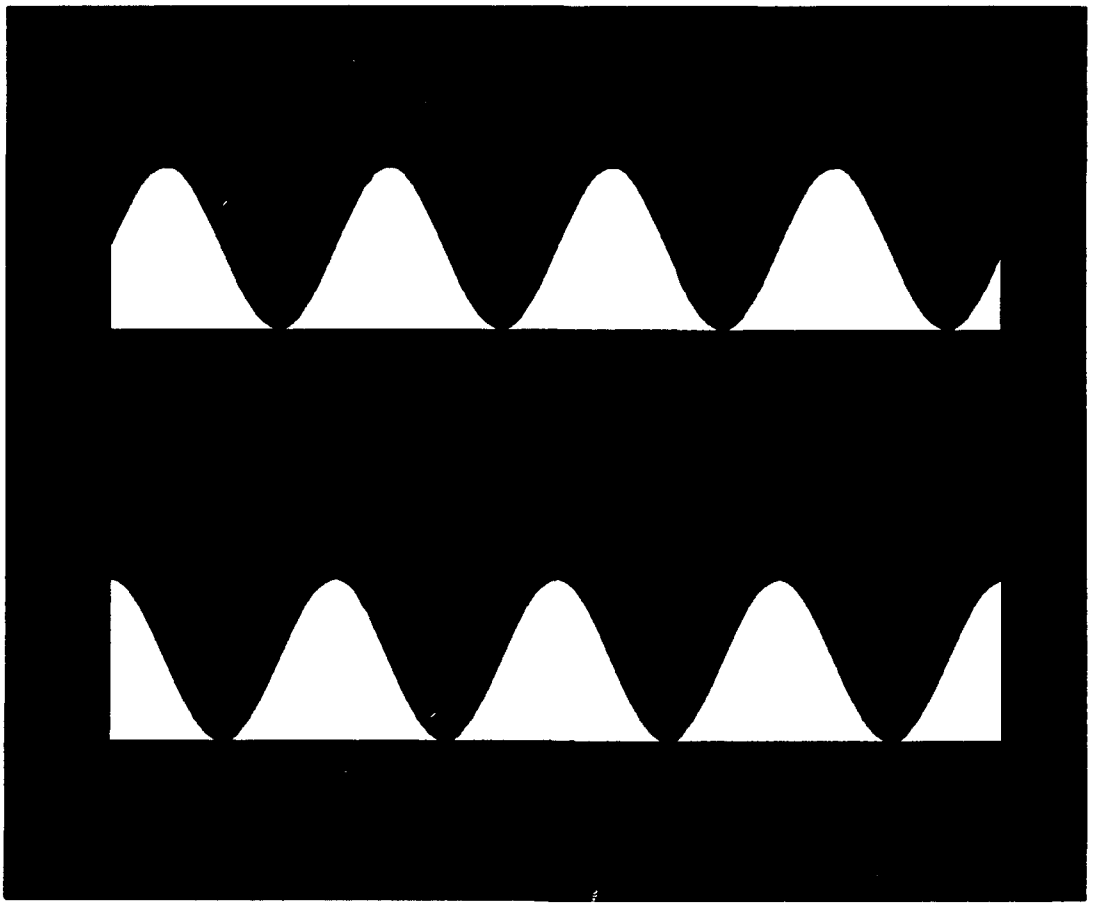

Figure 7 Optical Mask Design

c. Producing the Mask

The copy of the program that produces the mask is included in Appendix A. When the program is run, the amplitude of the desired curve and the period are specified by the user. The program then determines the solutions for the equation y=sin(x) and y=cos(x), and passes the solutions to an output file called MASK.DAT. This file is in Hewlett-Packard Graphics Language (HPGL) format, consisting of two-letter

mnemonic codes followed by numerical parameters. The overall size of the generated mask is 11x5 cm, as dictated by the dimensions of the film holder used to hold the mask in the optical setup. Once the mask was produced on paper, it was transferred onto a transparency for use during the experiment.

2. OPTICAL SETUP

The initial idea for the optical layout was to have two positive lenses with the same focal length f=10cm coaxial with each mask, LED and detector, as shown in Figure 8. The first lens would focus the light from the LED (located at 2f) down to a point on the mask (at a distance of 2f) and the second lens, also located a distance 2f from the mask, would refocus the light onto the detector. A narrow slit would be placed as close as possible to the mask to restrict the range of x values illuminated by the beams. This idea was rejected without testing because the amplitude of the sine wave on the mask would have to be extremely small for the focused light to cover the whole vertical dimension of the aperture.

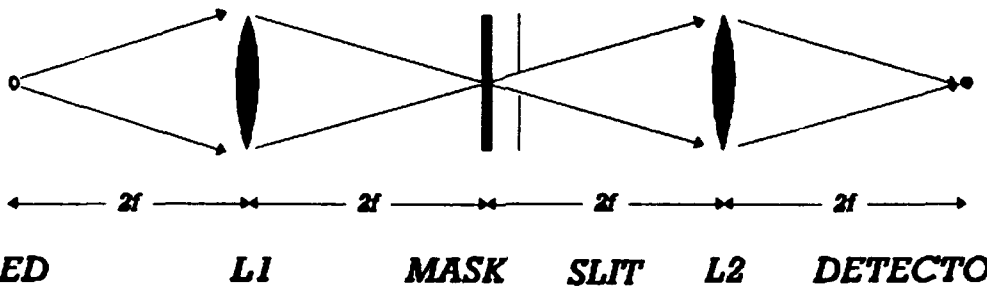

Figure 8 Initial Optical Layout

Figure 9 shows the final version of the layout. lens L_1 is located a distance f from the LED so that the light passing through L_1 is collimated. The light then passes through the mask, slit and L_2 (distances S_m, S_s and S_{L2} are arbitrary). Finally, L_2 focuses the light onto the detector located at a distance f.

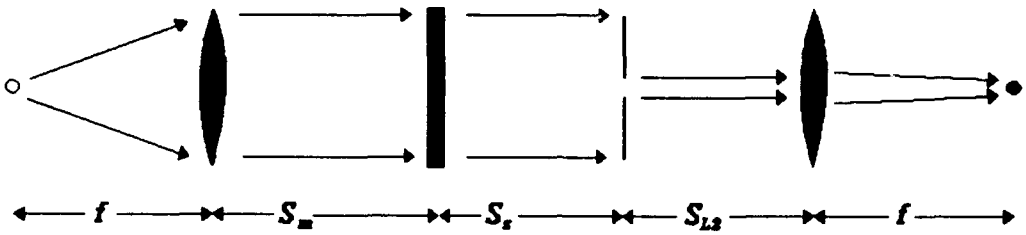

Figure 9 Final Optical Layout

The optical system was configured with the two channels stacked vertically, with channel one located 5cm above channel two. Figure 10 shows a photograph of the final optical layout.

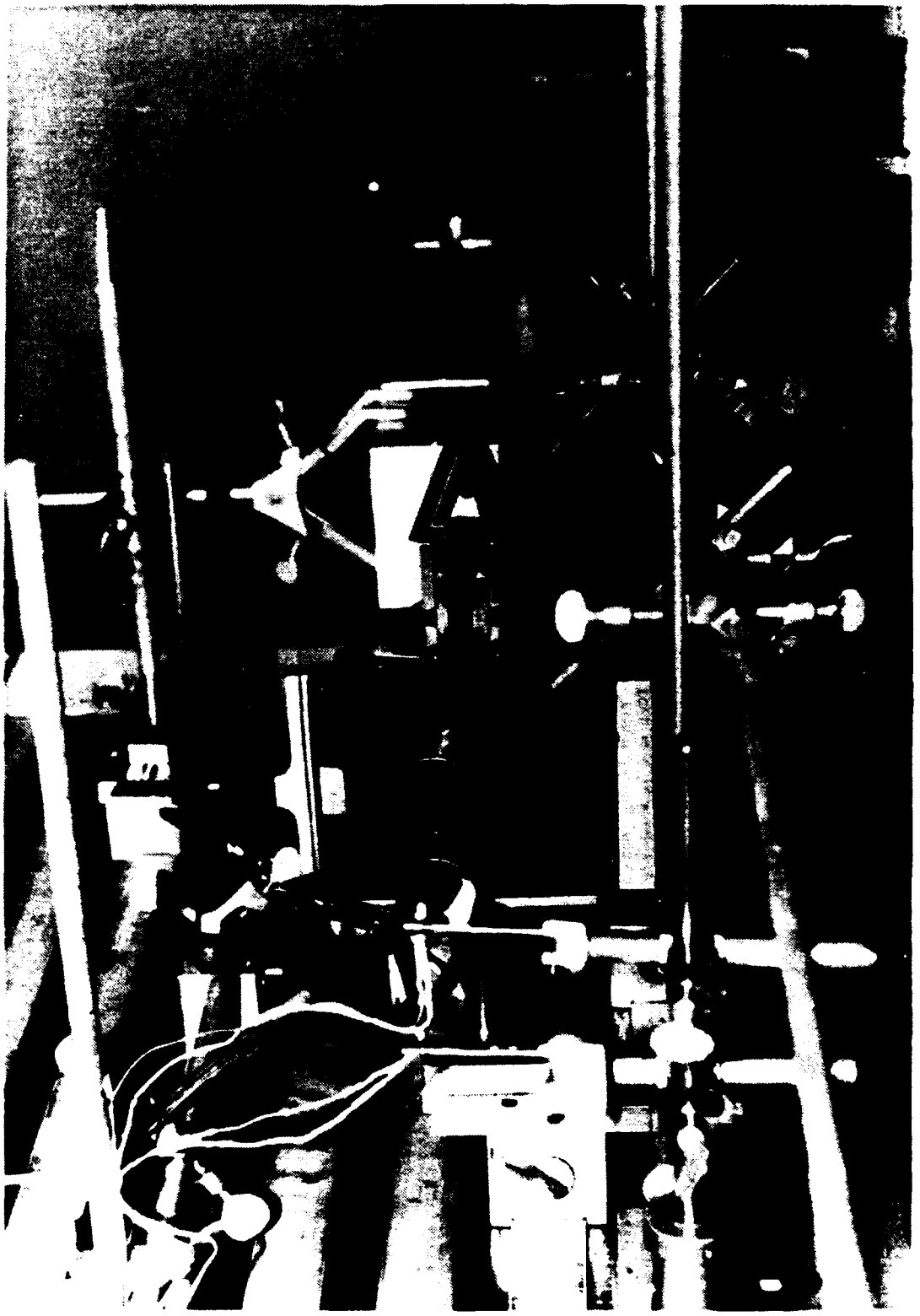

Figure 10 Photograph of Optical Layout

IV. RESULTS

A. INITIAL TESTING

1. Problems

Once the experimental setup was complete, the system was initially tested by connecting oscilloscope leads to the output of the voltage adder (IC U1, Figure 5) and to the reference signal. The first of these is the desired phase-encoded signal, while the second is the phase reference signal. The relative phases of the two signals were then visually compared as the position of the mask was changed.

The results of this test were disappointing. It was observed that the relative phase of the output signal shifted to a maximum of ninety degrees, as expected, when the mask was translated by one quarter wavelength. However, it then shifted back to zero instead of continuing to increase linearly. During discussions of possible causes for this behavior, the author and his advisor realized that the experimental configuration did not account for the DC signal terms caused by the fact that light intensities cannot be negative. Thus the two channels' intensities are actually proportional to $1+\sin(\omega t)$ and $1+\cos(\omega t)$ instead of $\sin(\omega t)$ and

cos(ωt). Consequently, the summed channel signals actually generate a voltage of the form

$$I \propto DC + \sin(\omega t) + \sin(x) + \cos(\omega t) + \cos(x) + \cos(\omega t - x), \quad (2)$$

rather than the one required by Equation (1).

2. Solution

The solution to this problem is straightforward. To eliminate the unwanted DC and low frequency (sin(x) and cos(x)) terms in Equation (2), a high pass filter was added downstream from the summation amplifier (see section II.C.2.). To eliminate the cos(ωt) and sin(ωt) terms, a second summing amplifier was included that would adjust the gain of the LED driving signals and add them together before subtracting that signal from the high-pass filter output signal, as discussed in section II.C.2 and shown in Figure 6.

B. NEXT ATTEMPT

With the above changes to the circuit completed, the system was ready for the next experimental trial. This time a Stanford Research Systems SR510 Lock-In Amplifier was included in the setup to monitor the relative phases. The output from the circuit was input into the lock-in amplifier as was the reference signal. The initial phase offset between the signals was nulled and a lock-in phase shift of ninety degrees was added in order to facilitate subsequent phase

measurements. The mask was moved in 0.1 inch increments, and the resulting phase differences were recorded.

1. Problem

The data from this experimental run are listed in Appendix B and plotted in Figure 11. The plot shows the observed relative phase difference (ϕ) vs the mask position (x). The straight line is a least squares fit of the data, and the curved line is included to show the periodicity of the data. This plot shows that the phase difference does increase with mask position, as expected, but there is also a significant periodic perturbation from linearity. The period of the perturbation is approximately equal to the period of the mask.

2. Solution

Possible causes for this periodic anomaly were then investigated. The initial belief was that it was due to a gain mismatch between the two signal channels. If there was indeed a gain mismatch, the summed signals would be $A\cos(\omega t)\cos(x)$ and $B\sin(\omega t)\sin(x)$, with $A \neq B$, and the trig identity (Equation (1)) would not work. Hence, it was decided to check for and to minimize any disparity with the gains.

The first place that the gains were adjusted was at the voltage adder IC U1, Figure 6. The output signal from

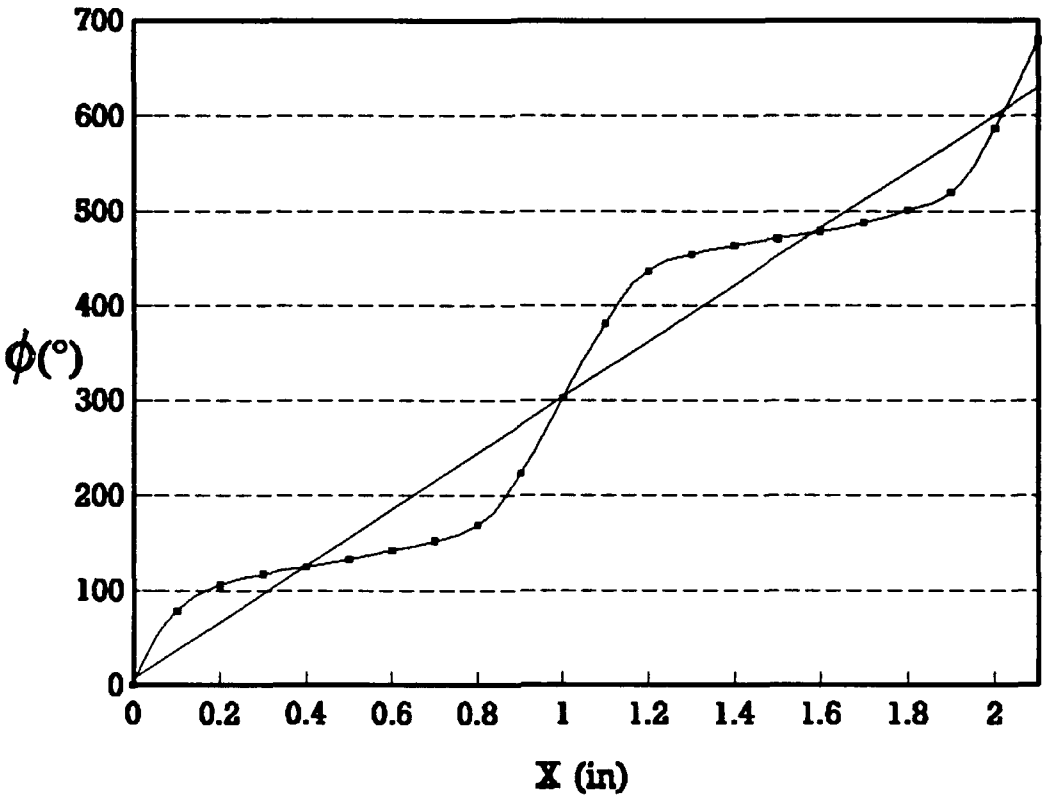

Figure 11 Phase vs Position for the Initial Data Set

detector channel one[1] was connected to the voltage adder and the adder's channel two input was grounded. The amplitude of channel one was measured with the oscilloscope and recorded. Then channel two was connected to the detector, channel one was grounded and the amplitude of channel two was adjusted to match that of channel one.

---

[1]Throughout this thesis, channel one is always the top optical system, and is considered to be the cos(ωt)cos(x) term, while channel two is the sin(ωt)sin(x) term. This distinction is completely arbitrary.

The only other point in the circuit where a gain mismatch could possibly be a problem was at the voltage adder IC U3A in Figure 6, where the reference signals, sin(ωt) and cos(ωt), are subtracted out (Equation (2)). Channel two in the signal processing circuit was initially grounded, and only one reference signal was connected to the adder. The output of the adder was connected to the oscilloscope. The position of the mask was adjusted until the signal measured on the scope was at half its maximum value, at which point the mask was at x=0 and the only term left in Equation (2) was cos(ωt). The reference signal for channel one was then reintroduced to the adder and its gain adjusted until the summed output signal was minimized while maintaining equality between the reference signal and the detector signal. The process was then repeated for channel two.

C. THIRD ATTEMPT

After the gains on the various circuit elements were adjusted, a second data set was collected. For this run, the mask was initially placed in a position so that when x=0, channel 1 was maximal. The results are listed in Appendix C and plotted in Figure 12.

1. Problems

The plot in Figure 12 shows that, although the amplitude of the periodic anomaly is reduced from its previous level, it is still present. It can be seen that the

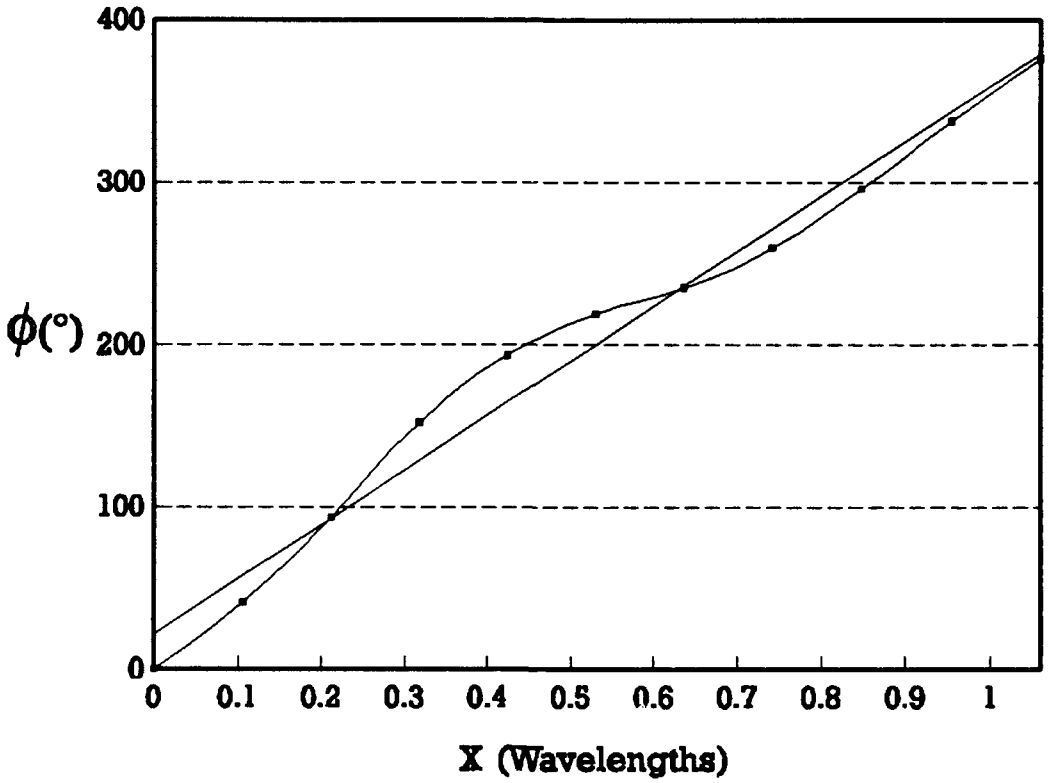

Figure 12 Phase vs Position for the Second Data Set

periodicity of the perturbation is still the same as the periodicity of the mask. The next cause of this periodicity to be investigated was a possible mechanical misalignment of the optical elements themselves.

2. Investigation

The potential for misalignment was examined by measuring the voltage output of the two detector channels. The mask was moved in increments of 0.1" and the channel voltages were read directly from the oscilloscope. When plotted the data should be of the functional form 1+cos(x) for

channel one and 1+sin(x) for channel two, if the signal gains and mechanical alignment are perfect. The actual results are listed in Appendix D, while Figure 13 is a plot of the data. The expected curves are shown by the solid and dotted lines: the solid line indicates the curve 1+cos(x) while the dotted line indicates 1+sin(x) (both curves are modified to match the amplitude and offset of the data). It shows that, although channel one was approximately of the form 1+cos(x), channel two showed a significant departure from the curve 1+sin(x). This indicates that there was indeed a geometric problem with the setup of the optical elements.

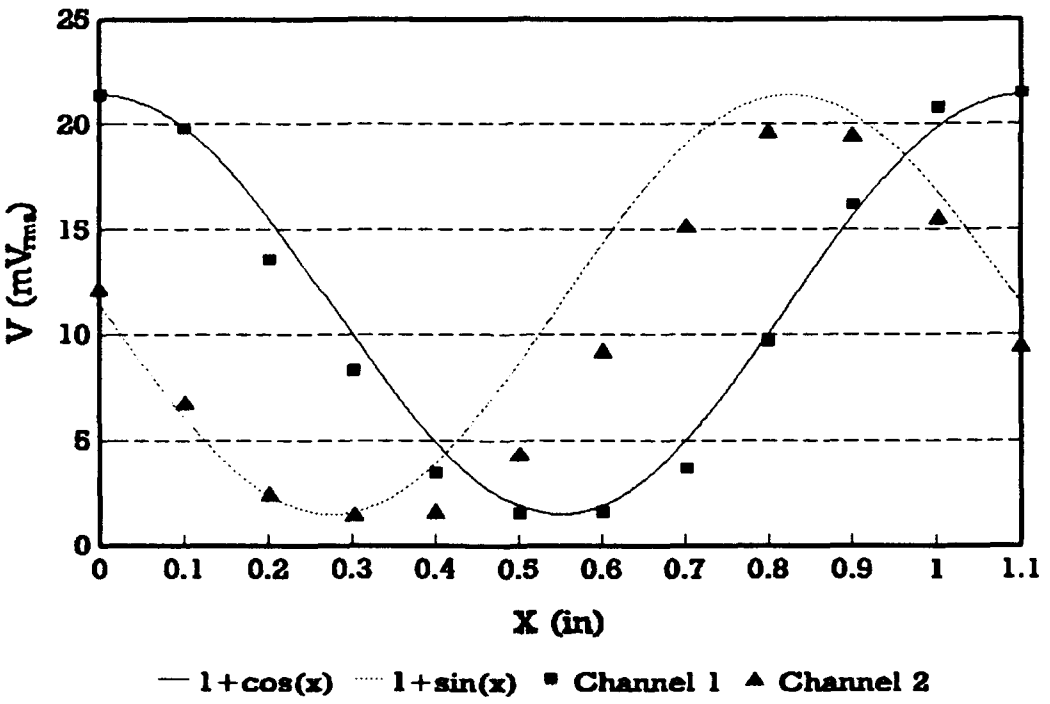

Figure 13 Detector Voltage vs Mask Position Prior to Realignment of Optical Elements

3. Solution

The misalignment problems were easily reduced by realigning the optical elements as accurately as possible using calipers and a level. After the realignment was completed, the circuit amplifier gains were readjusted as described above in section IV.B.2. The test described in section IV.C.2 was run again and the results are plotted in Figure 14 (the data are listed in Appendix E). The solid line indicates A[1+cos(x)] and the dotted line B[1+sin(x)] were the constants A and B were added to match the amplitudes of the data. These results are much closer to expectations, thereby proving that precise mechanical alignment is mandatory for these types of experiments.

D. FINAL EXPERIMENT

Upon completion of the geometric realignment and adjustment of the amplifier gains, a final set of data was taken. A Mitutoyo Corp Code 500-351 digital caliper, accurate to ±0.01mm, was used to measure the displacement of the optical mask. Measurements were made at mask displacement intervals of 0.5mm. The phase was once again measured with the lock-in amplifier.

The mask was displaced a total of 32mm and the caliper was checked several times to ensure that it stayed properly calibrated during the run. Also, the reproducability of the data was tested by moving the mask back to a position that had

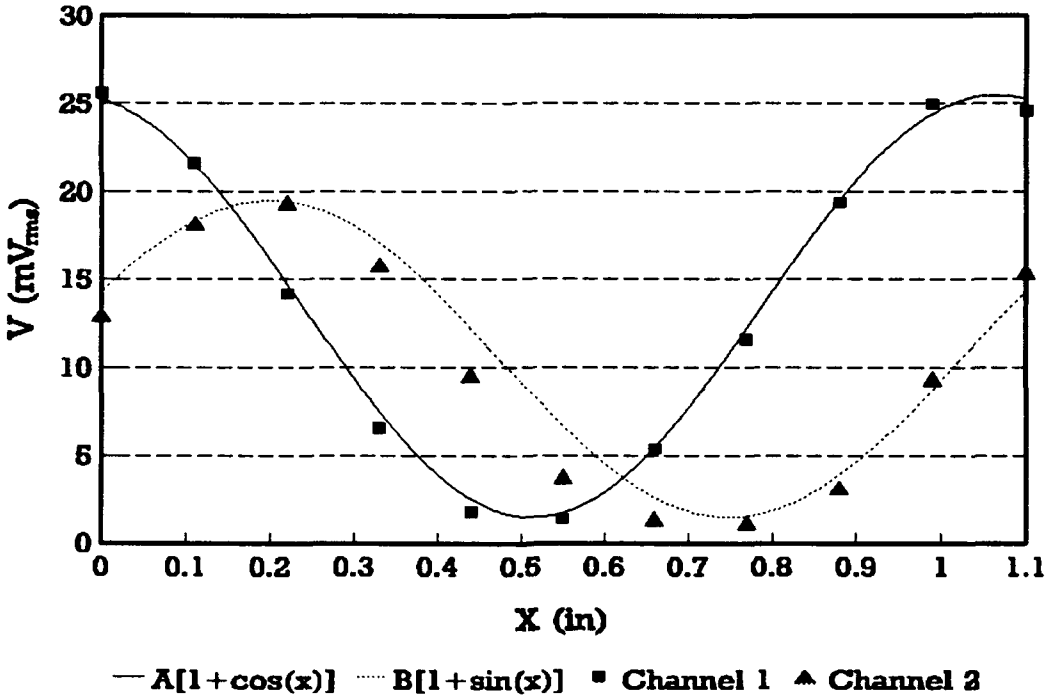

Figure 14 Detector Voltage vs Mask Position After Realignment of the Optical Elements

already been measured and comparing the phase difference with the previously measured value. It was determined that the phase data was reproducible within ±0.3°. The data are recorded in Appendix F and graphed in Figure 15.

The periodic perturbation is still present, but it is not as pronounced as in preceding trials. It is believed that the data is acceptable given the shortcomings of the experimental apparatus.

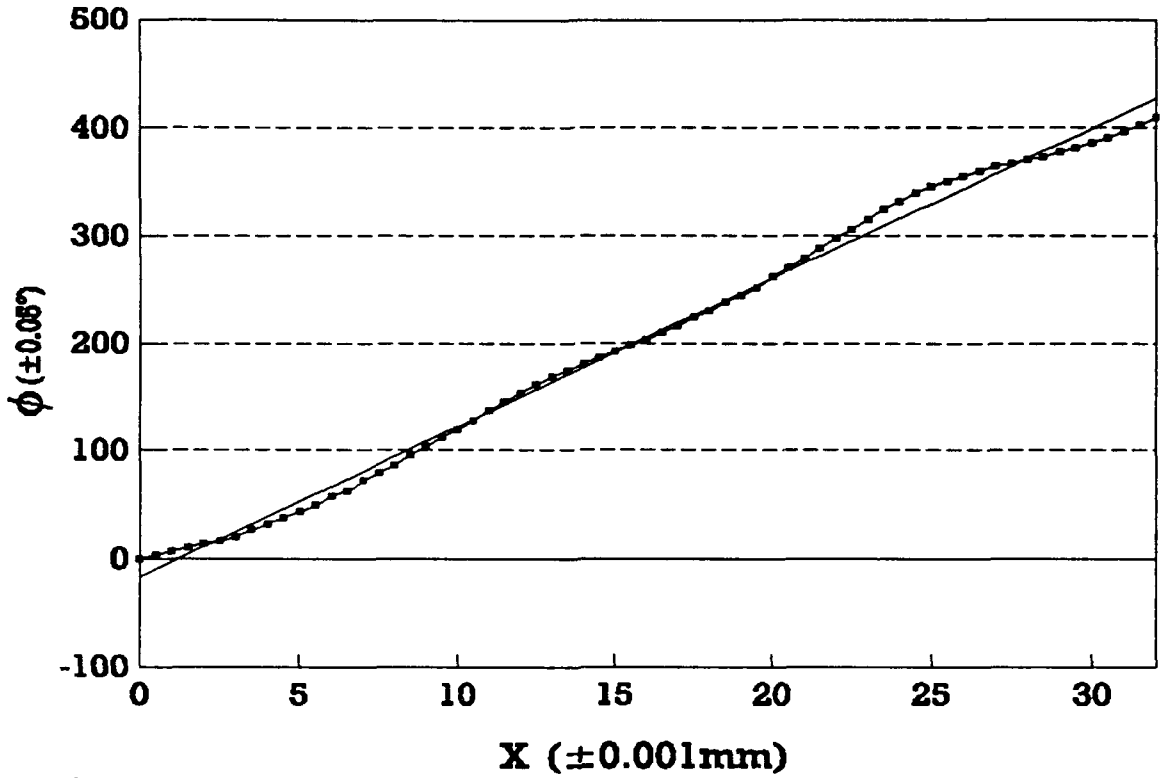

Figure 15 Graph of Phase vs Position for Final Data Set

E. ANALYSIS

1. Checking the Phase Relationship of the Driving Signals

A possible source for the remaining periodic discrepancy was thought to be an extraneous phase shift δ between the two LED driving signals. These two signals were connected directly to the lock-in amplifier, and the phase difference between them was measured. The results of this test disclosed that the phase difference is in fact $\Delta\phi=91.9\pm0.1°$ giving a value for δ of 1.9°.

This extra phase δ is of some concern. Because of its presence, the summation is not the desired summation as stated in Equation (1), but is rather

$$\sin(\omega t)\sin(x)+\cos(\omega t+\delta)\cos(x). \tag{3}$$

By introducing the trig identity

$$\cos(\omega t+\delta)=\cos(\omega t)\cos(\delta)-\sin(\omega t)\sin(\delta), \tag{4}$$

to Equation (3), the second term can be rewritten as

$$\cos(\omega t)\cos(x)\cos(\delta)-\sin(\omega t)\sin(\delta)\cos(x) \tag{5}$$

By using small angle approximations, $\sin(\delta)\approx\delta$ and $\cos(\delta)\approx 1$, Equation (3) becomes,

$$\sin(\omega t)\sin(x)+\cos(\omega t)\cos(x)-\delta\sin(\omega t)\cos(x). \tag{6}$$

To determine the overall effect of the extraneous phase shift δ, the measured signal is assumed to be $\cos(\omega t-\Delta)$ where Δ is the actual measured phase difference. This can be rewritten as

$$\cos(\omega t-\Delta)=\cos(\omega t)\cos(\Delta)+\sin(\omega t)\sin(\Delta). \tag{7}$$

Comparing the right hand side of this equation to Equation (6) gives the following results,

$$\begin{aligned}\cos(\Delta)&=\cos(x)\\ \sin(\Delta)&=\sin(x)-\delta\cos(x).\end{aligned} \tag{8}$$

And finally, solving Equations (8) for Δ yields

$$\Delta = \tan^{-1}\left(\frac{\sin(x) - \delta\cos(x)}{\cos(x)}\right). \qquad (9)$$

If the residual electrical phase difference δ was indeed the cause for the periodic nonlinearity in the final data set (Figure 15), then plotting Δ vs x should result in a simulated phase curve similar to the actual experimental result. Such a plot, with δ=1.9°, is shown in Figure 16. This graph does show a periodic anomaly, however it is symmetric about the ideal linear curve while the actual experimental data is not. Therefore, although the phase difference δ must be a contributing factor in the periodic discrepancy in the measured data, it cannot be the only cause.

2. Further Investigation

Another possible cause is that the gain matching discussed in section IV.B.2. was not completely successful. This would mean that the sin(ωt) and cos(ωt) terms were not fully subtracted out from Equation (2) and that the amplitudes of the summed signals in Equation (1) were not identical. If this is true, then the signal being measured, after the high pass filter, is

$$A\sin(\omega t) + B\cos(\omega t) + C\sin(\omega t)\sin(x) + D\cos(\omega t)\cos(x) + \delta\sin(\omega t)\cos(x) \qquad (10)$$

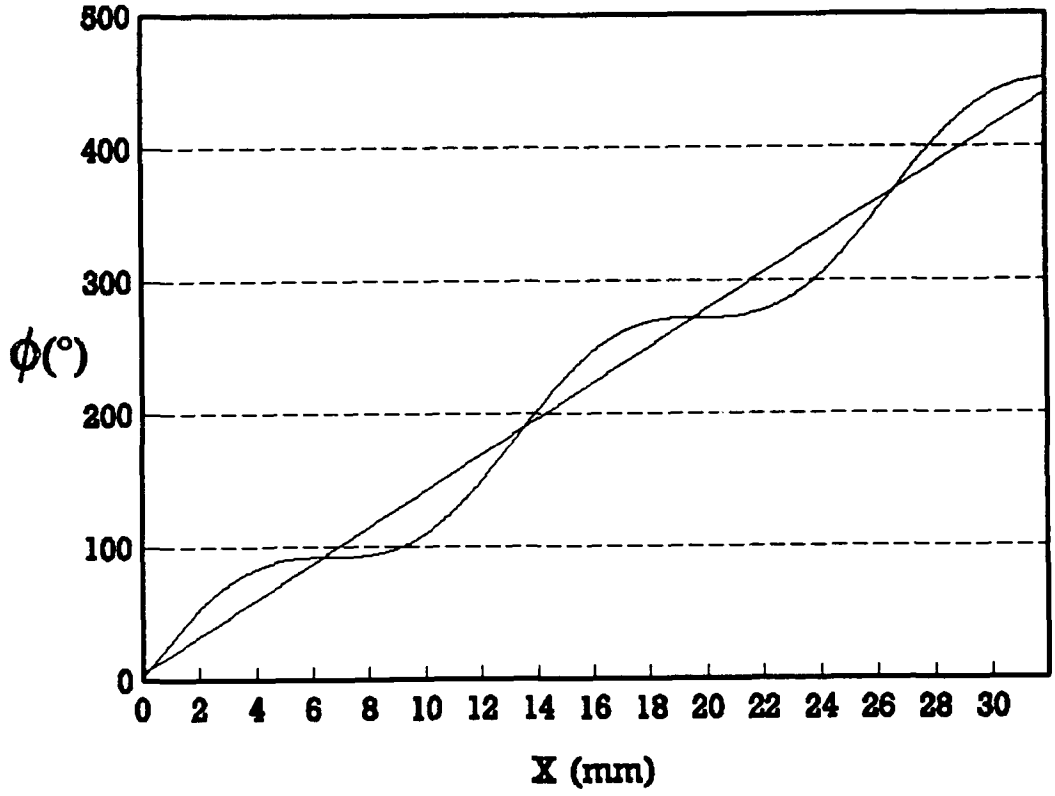

Figure 16 Simulated Phase Curve for δ=1.9°

Which can be written as

$$\sin(\omega t)\,[A+C\sin(x)+\delta\cos(x)]+\cos(\omega t)\,[B+D\cos(x)] \qquad (11)$$

Assuming that this equation corresponds to $\cos(\omega t-\Delta)$, and comparing it to the right hand side of Equation (7) gives

$$\cos(\Delta)=B+D\cos(x), \qquad (12)$$

and

$$\sin(\Delta)=A+C\sin(x)+\delta\cos(x). \qquad (13)$$

By dividing Equation (13) by Equation (12), it is possible to solve for Δ:

$$\tan(\Delta) = \frac{A + C\sin(x) + \delta\cos(x)}{B + D\cos(x)}. \qquad (14)$$

To determine the coefficients A, B, C, and D, it is necessary to perform a least-squares fit on the data [Ref. 9]. To simplify matters, a least-squares fit on tan(Δ) vs tan(x) was attempted. Carrying out the differentiation on the function and plugging into the least-squares fit formula gives the following system of four equations in four unknowns:

$$\sum_I \frac{A + B\sin(x_i) + \delta\cos(x_i)}{[C + D\cos(x_i)]^2} - \sum_I \frac{f_i}{C + D\cos(x_i)} = 0 \qquad (15)$$

$$\sum_I \frac{[A + B\sin(x_i) + \delta\cos(x_i)]\sin(x_i)}{[C + D\cos(x_i)]^2} - \sum_I \frac{f_i \sin(x_i)}{C + D\cos(x_i)} = 0 \qquad (16)$$

$$\sum_I \frac{[A + B\sin(x_i) + \delta\cos(x_i)]^2}{[C + D\cos(x_i)]^3} + \sum_I \frac{f_i[A + B\sin(x_i) + \delta\cos(x_i)]}{[C + D\cos(x_i)]^2} = 0 \qquad (17)$$

$$\sum_I \frac{[A + B\sin(x_i) + \delta\cos(x_i)]^2\cos(x_i)}{[C + D\cos(x_i)]^3} + \sum_I \frac{f_i[A + B\sin(x_i) + \delta\cos(x_i)]\cos(x_i)}{[C + D\cos(x_i)]^2} = 0 \qquad (18)$$

It was determined in discussions between the author and his advisor that solving this system of equations would involve techniques that are beyond the scope of this thesis. In order to further investigate the effect of gain mismatch another attempt at performing a partial least-squares fit was made, using a subset of Equations (15)-(18). By setting the constants A and B in Equation (10) equal to zero, the gain mismatch where the sin(ωt) and cos(ωt) terms (Equation (2))

are subtracted out is eliminated as a possible contribution to the phase anomaly. Equation (14) then reduces to $\tan(\Delta)=\alpha\tan(x)+\beta$ where $\alpha=C/D$ and $\beta=\delta/D$. Solving the resulting systems of two equations and plotting Δ versus x gives the results in Figure 17. The displayed behavior of the curve does not resemble the actual behavior of the measured data. Therefore it is concluded that any difference in amplitudes (C and D) between the $\sin(\omega t)\sin(x)$ and the $\cos(\omega t)\cos(x)$ terms in Equations (10) that may be present has negligible effect on the actual experiment. The observed anomaly is not produced by such amplitude mismatches.

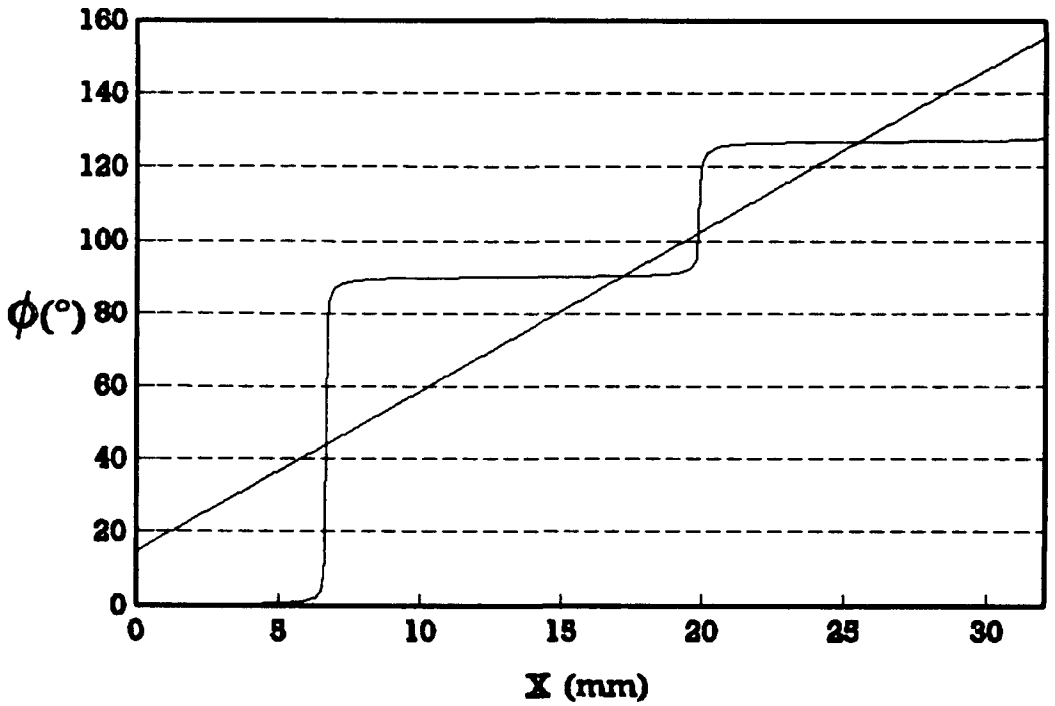

Figure 17 Simulated Phase Curve with Constants A=B=0 in Equation (10)

V. CONCLUSIONS/RECOMMENDATIONS

A. CONCLUSIONS

As stated in Chapter One, the goal of this thesis was to develop and to implement a proof-of-concept validation of the proposed electro-optical phase encoded position transducer. The plot in Figure 15 gives incontestable proof that the underlying concepts behind the technique are valid, although some residual problems remain. Further development is required before the technique can be incorporated into a working instrument for use in the infrared imaging system proposed by Davis.

B. RECOMMENDATIONS

The most difficult aspects of the project were the matching of the amplifier gains and the positioning of the optical elements. The mismatch of the amplifier gains was the most likely cause for the 1.9° phase error in the quadrature signals used to drive the LEDs. It probably also played a part in the nonlinearity of the final data. Possible error in the alignment of the optical elements may also have contributed to the observed nonlinearity.

It is recommended that, in future designs, higher precision electrical components be used in all circuits. This would eliminate the residual phase error as well as make matching the amplifier gains more stable and precise.

A complete least-squares fit of the data using linear programming techniques on Equations (10) should be conducted to determine the significance of the amplifier gain problems in the final results, with corrective action taken as described above.

The problem of alignment of the optical elements was a function of the equipment available to the author. Although great care will need to be taken in future designs to ensure the alignment is accurate, this should not be a major problem when using more precise opto-mechanical micropositioning equipment.

APPENDIX A

```
/*  Program THESPLOT

    Written by Lt Gary R Parriott, USN

    This program will draw an optical mask consisting of a
sine wave and a cosine wave such that the sine wave is two
inches above the cosine.  The areas under the curve will be
white, while the background areas (above the curves) will be
black.  The mask will be surrounded by a black window.  */


#include <stdio.h>
#include <math.h>

int main(void)
{
    /* Variable Declaration*/

    float A,x,x0,y,xscl,yscl;
    double PI=3.14159;
    int x1,y0,y1,y2,y3,y4,period;
    FILE *out;


    /* Open file named mask.dat in default directory and
        return error if not allowed */

    if    ((out=fopen("mask.dat","wt"))==NULL)    printf("No
    File/n");

    /* Enter the amplitude and number of periods required. */

    printf("Enter the number of periods desired.\n");
    scanf("%d", &period);
    printf("Enter  the  amplitude  of  the  Sine  waves  in
    centimeters.\n");
    scanf("%f", &A);


    /* Determine the values of the variables not designated by
    the user */

    xscl=4400/(2*period);  /* Scales the X coordinate */
    yscl=A*400;            /* Scales the Y coordinate */
```

```
y1=6184;          /* Sets the upper edge of the window */
y2=5000-yscl-10;   /* Sets the lower edge of the Sine */
y3=2968-yscl-10;  /* Sets the lower edge of the Cosine */
y4=1784;          /* Sets the lower edge of the window */


/* Initialize plotter, set up initial parameters */

fprintf(out,"%s","IN;PT0.7;SP1;GM12752;");
fprintf(out,"%s","PU3000,5000;");
fprintf(out,"%s","PM0;PA;PD;");


/* Determine coordinates of Sine wave for polygon */

for (x=0;x<=4400;x=x+25)
{
    x0=x*PI/xscl;
    y=sin(x0);x1=(int)x+3000;y0=(int)(yscl*y)+5000;
    fprintf(out,"%s%d%s%d%s","PD",x1,",",y0,";");
}


/* Define, fill and plot rest of polygon */

fprintf(out,"%s%d%s%d%s","PD7400,",y1,";PD3000,",y1,";");
fprintf(out,"%s","PM2;FP;EP;");


/* Reset parameters for new polygon */

fprintf(out,"%s","PU3000,2968;");
fprintf(out,"%s","PM0;PA;PD;");


/* Determine coordinates of Cosine wave for polygon */

for (x=0;x<=4400;x=x+25)
{
    x0=x*PI/xscl;
    y=cos(x0);x1=(int)x+3000;y0=(int)(yscl*y)+2968;
    fprintf(out,"%s%d%s%d%s","PD",x1,",",y0,";");
}


/* Define, fill and plot rest of polygon */

fprintf(out,"%s%d%s%d%s","PD7400,",y2,";PD3000,",y2,";");
fprintf(out,"%s","PM2;FP;EP;");
```

```
        /* Define and fill rectangles to finish plot */

        fprintf(out,"%s%d%s%d%s","PU2500,",y4,";RA3000,",y1,";");
        fprintf(out,"%s%d%s%d%s","PU3000,",y4,";RA7400,",y3,";");
        fprintf(out,"%s%d%s%d%s","PU7400,",y4,";RA7800,",y1,";");


        /* End plotting routine */

        fprintf(out,"%s","SP0;PG;");


        /* Close file and end program*/

        fclose(out);
        return;
    }
```

APPENDIX B

Phase vs Position for the Initial Data Set
Plotted in Figure 11

Position ($x \pm 0.001$")	Phase ($\phi \pm 0.1°$)
0.000	0.0
0.100	78.3
0.200	106.0
0.300	117.8
0.400	125.4
0.500	133.1
0.600	142.6
0.700	152.7
0.800	169.9
0.900	223.1
1.000	303.0
1.100	382.0
1.200	437.2
1.300	454.6
1.400	463.6
1.500	471.2
1.600	479.0
1.700	488.0
1.800	501.3
1.900	520.4
2.000	587.4
2.100	679.3

APPENDIX C

Phase vs Position for the Second Data Set
Plotted in Figure 12

Position ($x \pm 0.001$")	Phase ($\phi \pm 0.1°$)
0.000	0.0
0.106	41.0
0.212	93.6
0.318	151.8
0.424	193.6
0.530	219.2
0.636	235.1
0.742	259.9
0.848	295.7
0.954	337.7
1.06	376.1

APPENDIX D

Detector Voltage vs Mask Position
Prior to Realignment of Optical Elements
Plotted in Figure 13

Position (x ± 0.001")	Channel 1 Voltage (mV_{rms})	Channel 2 Voltage (mV_{rms})
0.000	21.4	12.2
0.154	19.8	6.8
0.254	13.6	2.5
0.354	8.3	1.5
0.454	3.5	1.65
0.554	1.55	4.4
0.654	1.6	9.25
0.754	3.7	15.2
0.854	9.7	19.7
0.954	16.2	19.5
1.054	20.8	15.6
1.154	21.5	9.5

APPENDIX E

Detector Voltage vs Mask Position
After Realignment of Optical Elements
Plotted in Figure 14

Position (x ± 0.001")	Channel 1 Voltage (mV_{rms})	Channel 2 Voltage (mV_{rms})
0.00	25.6	13.0
0.11	21.6	18.2
0.22	14.2	19.4
0.33	6.6	15.8
0.44	1.8	9.6
0.55	1.4	3.8
0.66	5.4	1.4
0.77	11.6	1.2
0.88	19.4	3.2
0.99	25.0	9.4
1.10	24.6	15.4

APPENDIX F

Phase vs Position
Final Data Set
Plotted in Figure 15

Position (x ± 0.01mm)	Phase (ϕ ± 0.3°)
0.0	0.0
0.5	4.0
1.0	6.6
1.5	10.4
2.0	14.2
2.5	16.7
3.0	20.0
3.5	26.6
4.0	31.7
4.5	37.4
5.0	43.2
5.5	49.1
6.0	57.7
6.5	62.1
7.0	71.6
7.5	79.4
8.0	85.8
8.5	95.7
9.0	103.3
9.5	111.7
10.0	119.0
10.5	128.0

Position (x ± 0.01mm)	Phase (ϕ ± 0.3°)
11.0	137.2
11.5	145.2
12.0	153.7
12.5	162.0
13.0	169.2
13.5	174.8
14.0	181.2
14.5	186.2
15.0	192.2
15.5	198.3
16.0	203.0
16.5	210.2
17.0	216.0
17.5	224.0
18.0	229.9
18.5	238.6
19.0	244.9
19.5	251.8
20.0	262.1
20.5	270.7
21.0	279.0
21.5	288.2
22.0	297.5
22.5	306.1
23.0	314.9
23.5	324.5
24.0	332.1
24.5	339.7
25.0	346.2

Position (x ± 0.01mm)	Phase (ϕ ± 0.3°)
25.5	350.8
26.0	355.9
26.5	360.5
27.0	364.4
27.5	367.4
28.0	370.6
28.5	373.5
29.0	377.7
29.5	381.5
30.0	386.1
30.5	391.1
31.0	397.1
31.5	402.8
32.0	409.3

LIST OF REFERENCES

1. Davis, D. S., "A New Technique for Efficient Multiplex Imaging and Imaging Spectroscopy," Paper in Preparation.

2. McKenzie, R. H., *A Demonstration of the Use of Walsh Functions for Multiplexed Imaging*, Masters Thesis, Naval Postgraduate School, Monterey Ca., 1990.

3. Musselman, B. J., *A Study of the Diffraction Behavior and Resolution Criteria for Pattern Recognition for a Proposed Multiplexed Imaging Technique*, Masters Thesis, Naval Postgraduate School, Monterey Ca., 1991.

4. Connes, P., and Michel, G., "Astronomical Fourier Spectrometer," *Applied Optics*, v. 14, p.2067, 1975.

5. Davis, D. S., and others, "Infrared Fourier Spectrometer for Airborne and Ground-Based Astronomy," *Applied Optics*, v. 19, p.4138, 1980.

6. Horowitz, P., and Hill, W., *The Art of Electronics*, 2nd ed., pp. 286-287, Cambridge University Press, 1989.

7. Lancaster, D., *TTL Cookbook*, 1st. ed., Howard W. Sams & Co., Inc., 1974.

8. Lancaster, D., *Active-Filter Cookbook*, 1st ed., Howard W. Sams & Co., Inc., 1978.

9. Taylor, John R., *An Introduction to Error Analysis*, pp. 153-168, Oxford University Press, 1982.

INITIAL DISTRIBUTION LIST

1. Defense Technical Information Center — 2
   Cameron Station
   Alexandria, VA 22304-6145

2. Library, Code 52 — 2
   Naval Postgraduate School
   Monterey, CA 93943-5002

3. Professor K.E. Woehler, Code PH/Wh — 1
   Chairman, Department of Physics
   Naval Postgraduate School
   Monterey, CA 93943-5000

4. Assoc. Professor D.S. Davis, Code PH/Dv — 2
   Department of Physics
   Naval Postgraduate School
   Monterey, CA 93943-5000

5. Assoc. Professor D.D. Cleary, Code PH/Cl — 1
   Department of Physics
   Naval Postgraduate School
   Monterey, CA 93943-5000

6. Department of Physics Library — 2
   Naval Postgraduate School
   Monterey, CA 93943-5000

7. Lt. G.R. Parriott, USN — 2
   902 Banbury Road
   Mundelein, IL 60060